Chapter 4

Upper Ocean Physical and Biological Response to Typhoon Cimaron (2006) in the South China Sea

Yujuan Sun, Jiayi Pan and William Perrie

Additional information is available at the end of the chapter

http://dx.doi.org/10.5772/64099

Abstract

The physical dynamic and biological response processes to Typhoon Cimaron (2006) in the South China Sea are investigated through the three-dimensional Regional Ocean Modeling System (ROMS). For sea surface temperatures, ROMS achieves a correlation of more than 0.84, with respect to satellite observations, indicating a generally high level of skill for simulating the sea surface temperature variations during Typhoon Cimaron (2006). However, detailed analysis shows that ROMS underestimates the sea surface temperature cooling and mixed layer deepening because of insufficient mixing in the model simulations. We show that the simulation accuracy can be enhanced by adding a wave-induced mixing term (B_V) to the nonlocal K-profile parameterization (KPP) scheme. Simulation accuracy is needed to investigate nutrients, which are deeply entrained to the oligotrophic sea surface layer by upwelling induced by Typhoon Cimaron, and which plays a remarkable role in the subsequent phytoplankton bloom. Simulations show that the phytoplankton bloom was triggered 5 days after the passage of the storm. The surface ocean was restored to its equilibrium ocean state by about 10–20 days after the typhoon's passage. However, on this time-scale, the resulting concentrations of nitrate and chlorophyll *a* remained higher than those in the pre-typhoon equilibrium.

Keywords: Typhoon Cimaron, SST cooling, mixed layer deepening, phytoplankton bloom, wave-induced mixing

1. Introduction

Tropical cyclones are extremely high wind events generated over tropical oceans, capable of producing strong mixing and entrainment, transient upwelling, and internal waves. The

response of upper ocean water to typhoons can be conventionally divided into two stages, the forcing stage and the relaxation stage in [1, 2]. In the first stage, potential energy is injected into the surface ocean by strong typhoon winds. Two significant physical phenomena caused by typhoons are the mixed layer deepening and sea surface temperature cooling in the wake of the storm. Warm water in the ocean surface layers is transported outward from the typhoon center and downward to depths ranging from tens of meters to beyond a hundred meters; cold water upwells from the deeper ocean along the typhoon's passage [3]. The current velocity in the surface mixed layer can reach 2 m s^{-1} or more, responding to the intensity of the tropical storm winds [2]. The relaxation stage following a typhoon's passage is primarily due to the inertial gravity oscillations excited by the storm in its wake, where the ocean adjusts towards a new geostrophic equilibrium state [1, 4–6]. The work of [7] concluded that the inertial oscillations are predominantly locally generated and the surface winds account for a large part of the energy and variability of such oscillations near the ocean surface. The theory of geostrophic adjustment was further reviewed in [8]. The latter theory, which describes the nature of the difference between the baroclinic and barotropic responses of the ocean to a moving storm as caused by the difference in the gravity wave speed, was first pointed out in [9]. The storm-induced oscillating wake is formed by the slow propagating, near-inertial gravity baroclinic waves, while the fast propagating barotropic waves produce a broad area of convergent depth-averaged currents with no discernible wake; the latter is determined entirely by the wind stress curl, with negligible effects due to the earth's rotation and ocean stratification [10]. The work of [11] confirmed that the mixed layer dynamics is associated with shear-induced entrainment mixing, and forced by near-inertial motions up to the third day after the passage of the storm.

Tropical storms also exert a strong influence on the oceanic chlorophyll *a* field and primary production in the ocean. Another important phenomenon triggered and enhanced by tropical cyclones is the phytoplankton bloom accompanied by nutrient pumping into the oligotrophic surface layer. Concentration of nitrate, phosphate, and chlorophyll *a* is observed to significantly increase after the occurrence of cyclonic disturbances [12]. In [13], after Typhoon Fengwong and Typhoon Sinlaku passed over the southern East China Sea in 2008, the in-situ particulate organic carbon flux was observed to experience a significant increase of about 1.7-fold and 1.5-fold, respectively, compared to the recorded (140–180 mg cm^{-2} d^{-1}) pre-typhoon concentration. The phytoplankton population growth was constrained by the light limitation and the grazing pressure. This increase of the surface chlorophyll *a* concentration might last 2–3 weeks before relaxing to pre-typhoon levels [14]. Because of the limitations imposed by in-situ point observations from ships or moored buoys along a typhoon's track, studies of the associated biological responses have become to more and more depend on the satellite observations. In the work of [15], satellite data are used as new evidence to quantify the contribution of tropical cyclones to enhance the ocean primary production. It was found that the peak of the chlorophyll *a* concentration enhancement tended to occur several days after the sea surface temperature cooling had achieved the maximum amplitude, after the typhoon's passage, see [16, 17]. The extended region and concentration of primary production bloom tend to vary in response to the translation speed and intensity of typhoon. Weak slow-moving typhoons can cause enhanced concentrations of chlorophyll *a*, while strong fast-moving typhoon tends to cause

http://dx.doi.org/10.5772/64099

more intense phytoplankton blooms over a larger geographic range, in the wake of the storm as discussed in [18]. Upwelling induced by tropical storms is within the region where the typhoon-induced enhancement of the chlorophyll *a* concentration occurs; please see [19]. The pre-existing cyclonic eddy is capable of strengthening the typhoon-induced nutrient pumping. However, the extent to which that upwelling contributes in the phytoplankton bloom is not clear yet. The development of biological models is helpful to investigate the relevant dynamic process of the nitrogen and carbon cycle in the ocean [20–22].

The ocean temperature cooling and mixed layer deepening caused by tropical storms, usually are underestimated in three-dimensional ocean model simulations, because of the insufficient mixing [23, 24]. Improvements of the mixing estimates in the simulation leading to more realistic and reliable simulations may solve this problem. After the potential energy injected into the mixed layer by tropical storms, wave dispersion spreads energy in both the vertical and meridional directions from the mixed layer [1]. Surface waves have been measured and simulated and shown to play a certain role on enhancing the turbulence in the subsurface layer [25, 26]. In the work of [24], a surface wave model was coupled to a three-dimensional ocean current model (POM), and some related estimates for transfer of momentum and wave energy are derived, assuming linear theory for vertically dependent wave motions. The effect of wave breaking on the simulation of sea surface temperatures and surface boundary layer deepening was investigated in [27]. A wave-induced vertical viscosity (B_V) term, as a function of wave number spectrum, was developed and applied in a global ocean circulation model [28, 29]. This surface wave-induced vertical viscosity term also has a key role on the simulation of sea surface temperature cooling and the mixed layer deepening after typhoon's passage.

In our study, a biological model is coupled to the three-dimensional Regional Ocean Modeling System (ROMS) to investigate both the physical and biological process of Upper Ocean in response to Typhoon Cimaron (2006) which occurred in the South China Sea. Typhoon Cimaron formed over the Pacific Ocean east of the Philippines on October 28, 2006, and then propagated westward, entering the South China Sea on October 30. Thereafter, Cimaron moved to the northwest part of the South China Sea and remained quasistationary during November 1–2, moving southwest on November 3, and finally dissipating near the Vietnamese coast on November 7. Both the mixed layer deepening and sea temperature cooling are underestimated in the model simulation, in comparison to reliable estimates of mixed layer deepened (about 104 m) on November 3 using a one-dimensional remote sensing model [30]. Therefore the wave-induced mixing term B_V is incorporated into ROMS model to improve the accuracy of the simulation.

2. Materials and methods

ROMS is utilized to simulate the processes of Typhoon Cimaron, which influenced the South China Sea from October 29 to November 7, 2006. The model region covers the whole South China Sea including 0°–30°N, 99°–130°E. There are 220 × 100 orthogonal curvilinear grids with the horizontal resolution varying at Δx (5.5–40 km) and Δy (3.6–37 km) and the minimum and

maximum depths are 5 m and 5000 m, respectively (**Figure 1**). There are 80 layers in the vertical direction using the *s*-coordinate formulation. The western boundary is closed and the other three open boundaries are defined by the radiation boundary condition.

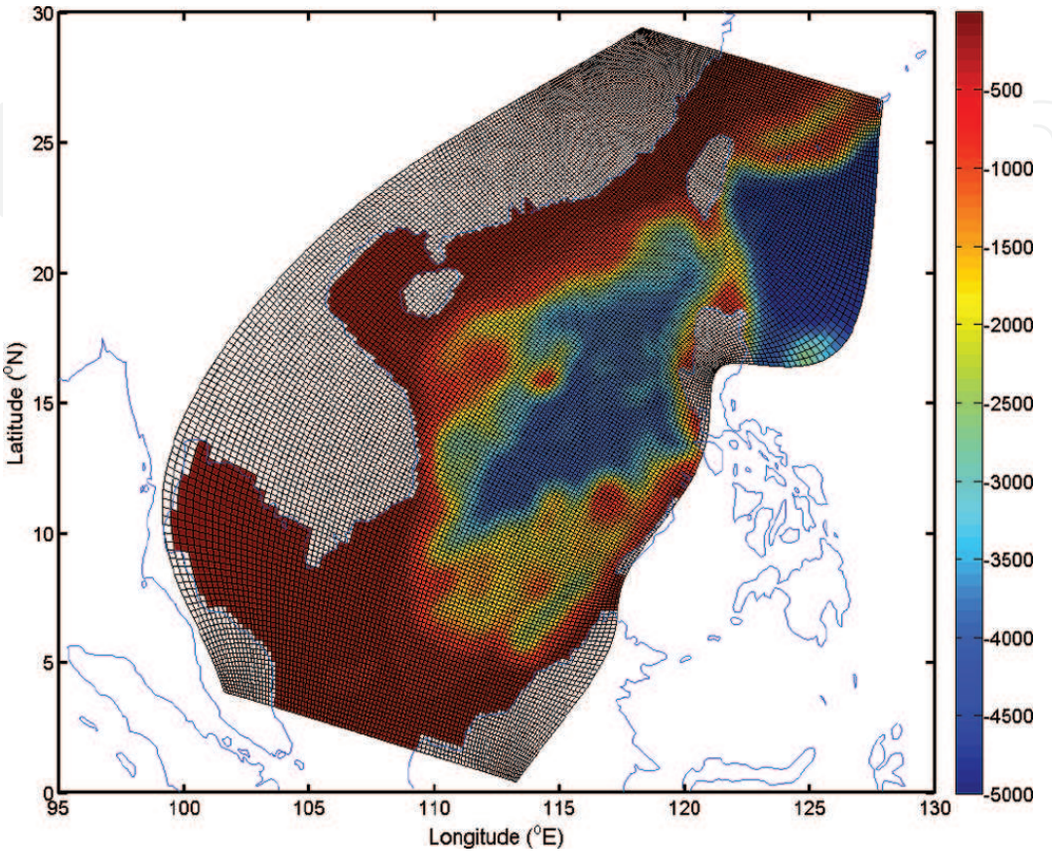

Figure 1. Model domain and grids, as well as bathymetry.

The initial temperature and salinity conditions are taken from the 1/4° grid climatological temperature and salinity analyses of October from WOA01 to represent the pre-typhoon conditions in the South China Sea, which was discussed by Carton and Giese [31]. The climatological monthly data have 24 standard levels with depths varying from 0 to 1500 m and the seasonal data have 33 standard levels with depths from 0 to 5500 m. As the maximum depth in the model is 5000 m, the climatological monthly data are applied in the upper 1500 m and the climatological seasonal data (autumn) are applied from 1500 to 5000 m. The initial current velocity is set to zero in this study.

The lateral boundary conditions for temperature, salinity, sea level and current velocities are obtained from the 5-day averages from the global simulations of the Simple Ocean Data Assimilation (SODA) dataset with horizontal resolution of 0.5° × 0.5° and 40 vertical layers [31]. The Kuroshio Current transport can be identified on the eastern boundary. The tidal amplitudes and phases used in this model are obtained from the TPXO Global Inverse solution database [32] with eight primary tide constituents (M2, S2, N2, K2, K1, O1, P1, and Q1) and two long-period constituents (Mf and Mm).

http://dx.doi.org/10.5772/64099

The daily wind stresses are obtained from QuikSCAT satellite data. The effect of heat flux is considered as the surface boundary for momentum, although the heat flux can be neglected under the extreme meteorological phenomena such as tropical cyclones. The daily heat fluxes are obtained from the Objectively Analyzed air-sea Fluxes (OAFlux) project which is an ongoing research and development project for global air-sea fluxes [33]. To present the climatological heating or cooling trends, we computed the surface boundary conditions for temperature and salinity involving relaxation to its observed values. Corrections are made for the net surface heat flux in the model simulations, as discussed in [34].

For the biological model, the surface chlorophyll *a* field data are estimated from the SeaWiFS climatological seasonal data, and the nitrate (NO_3) and oxygen are estimated from the monthly climatological database of WOA09 [35, 36]. The vertical structure of chlorophyll *a* is extrapolated from the surface chlorophyll *a* field using the Morel and Berthon [37] parameterization method. High concentrations of chlorophyll *a* are mostly distributed in coastal regions along the coastline of southern China and the Vietnam marginal continent, with values of over 1 mg cm^{-3}. By comparison, in the deep sea area, the concentration is less than 0.1 mg cm^{-3}. In most areas of the South China Sea, the NO_3 content is much smaller, less than 0.1 mmol Nm^{-3} in the deep ocean surface layer. The concentration of NO_3 increases with ocean depth. In the deep sea, with depths in excess of 800 m, the concentration of NO_3 can reach 40 mmol Nm^{-3}.

Both the total inorganic carbon (TIC) and total alkalinity are obtained from the Carbon Dioxide Information Analysis Center. The detailed data information is given in work et al. [38]. The climatological seasonal dataset is used to generate the initial and boundary conditions. Ammonium (NH_4), large and small detritus, and N-concentration are taken from the NO_3 estimates and multiplied by the respective ratios of 18/62, 0.1 and 0.1, respectively, while phytoplankton, zooplankton, large and small detritus, and C-concentration are taken from the chlorophyll *a* concentration multiplied by the respective ratios of 0.5, 0.2, 0.1, and 0.1, respectively.

3. Model validation

Two Optimally Interpolated (OI) SST daily products (including microwave plus infrared (MWIR) OI SSTs and microwave only TMI AMSRE SSTs) are used in comparisons with the simulated SSTs to validate the model accuracy. MWIR OI SST product is at 9 km resolution, while TMI AMSRE SST product is at 25 km resolution. The validation statistical parameters contain mean error (ME), mean absolute error (MAE), root-mean-square (RMS), and correlation coefficient (R). The formulas to calculate these statistical parameters are presented in [39].

The simulated SSTs (**Figure 2**) are compared with the satellite observations from October 30 to November 6. The validation region is set from 99°E to 120°E and from 0°N to 26°N. For validation of the simulation, the statistical parameters are displayed in **Table 1** for MWIR OI and **Table 2** for TMI AMSRE. The MEs of the simulated SSTs are less than 0.12°C, compared with the MWIR SSTs; for TMI AMSRE SSTs, the MEs are within 0.14–0.24°C. Negative signs indicate that the modelled SSTs are less than the observed SSTs. The MAEs are within the range

from 0.4°C to 0.6°C, and the RMS errors are less than 0.9°C. The correlation coefficients between the MWIR OI SST and simulated SST are over 87% from October 30 to November 6, while the correlation coefficients validated with TMI AMSRE SSTs are over 84%. The high values of the correlation coefficients indicate that the simulated SSTs are within a reasonable range. Therefore, we have demonstrated that ROMS can generally reproduce the processes of Typhoon Cimaron in the South China Sea.

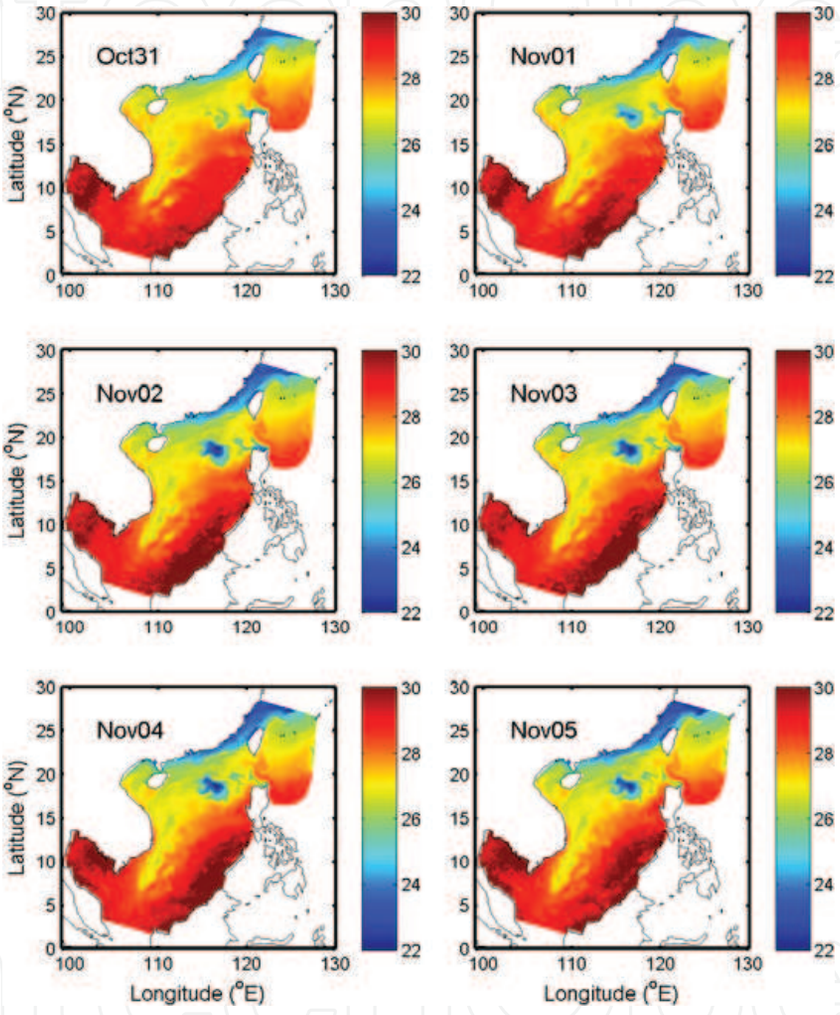

Figure 2. The simulated SSTs (unit: °C) from October 31 to November 5, 2006.

	Oct 30	Oct 31	Nov 1	Nov 2	Nov 3	Nov 4	Nov 5	Nov 6
ME (°C)	−0.12	−0.12	−0.09	−0.04	−0.01	−0.00	−0.09	−0.10
MAE (°C)	0.42	0.45	0.50	0.54	0.58	0.56	0.55	0.58
RMS (°C)	0.56	0.61	0.69	0.76	0.88	0.81	0.78	0.80
R	0.89	0.88	0.88	0.89	0.87	0.88	0.88	0.88

Table 1. Statistics of the simulated SSTs versus MWIR OI SSTs from October 30 to November 6, 2006.

http://dx.doi.org/10.5772/64099

	Oct 30	Oct 31	Nov 1	Nov 2	Nov 3	Nov 4	Nov 5	Nov 6
ME (°C)	−0.23	−0.24	−0.21	−0.14	−0.14	−0.17	−0.21	−0.16
MAE (°C)	0.41	0.44	0.48	0.53	0.53	0.49	0.46	0.46
RMS (°C)	0.53	0.58	0.71	0.77	0.78	0.71	0.68	0.67
R	0.87	0.86	0.84	0.87	0.88	0.89	0.89	0.90

Table 2. Statistics of the simulated SSTs versus TMI AMSRE SSTs from October 30 to November 6, 2006.

4. Results

4.1. Ocean temperatures

The ocean surface temperature distributions from October 31 to November 5, 2006 are shown in **Figure 2**. Cimaron entered the South China Sea on October 30, and the simulation of the typhoon-induced wake suggests that the apparent temperature depression started on October 31. The wake of the typhoon occurred within the region from 15°N to 20°N and from 114°E to 119°E. **Figure 3** shows the time series (daily) of the maximum SST decreasing in the typhoon-induced wake, located at 18.51°N and 116.45°E, relative to the pre-typhoon conditions on October 28. Although bias exists between these two satellite SST observations, both satellite SSTs display the same trend in their variations in the SST cooling amplitude in the wake. The

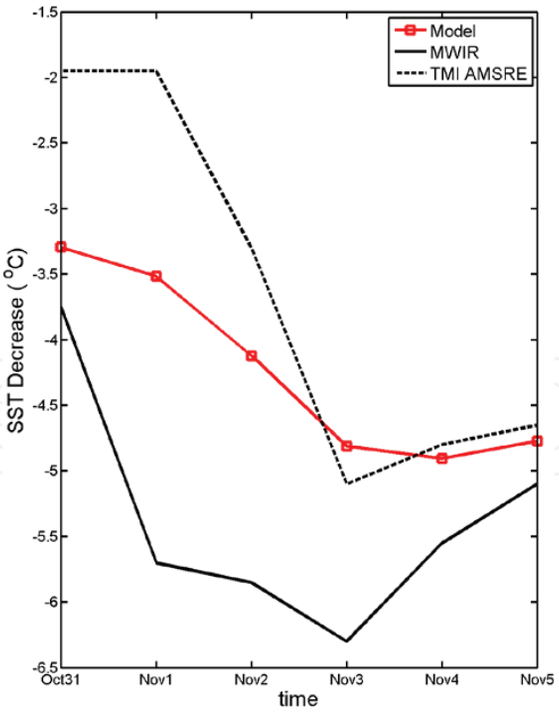

Figure 3. Maximum SST decrease in the typhoon wake from October 31 to November 5, 2006 (the red solid line with squares denotes the model results; the dash line denotes TMI AMSRE satellite observations; the solid line represents MWIR OI satellite observations).

observed SST decreased to an extremely low value on November 3, by which time the ocean was in the forcing stage. Starting from November 3, SSTs had begun to increase, which defines the beginning of the relaxation stage towards a new equilibrium state, with the injection of potential vorticity into the wake by the typhoon winds [1]. Comparing model results to these two satellite SSTs which show that the maximum amplitude of the SST cooling appeared on November 3, with values of 5.1°C for TMI AMSRE and 6.3°C for MWIR OI, the simulated maximum SST cooling was 4.8°C on November 4 (**Figure 3**). Thus, the relaxation of surface temperature in the wake after the typhoon's passage is clearly underestimated in our simulations.

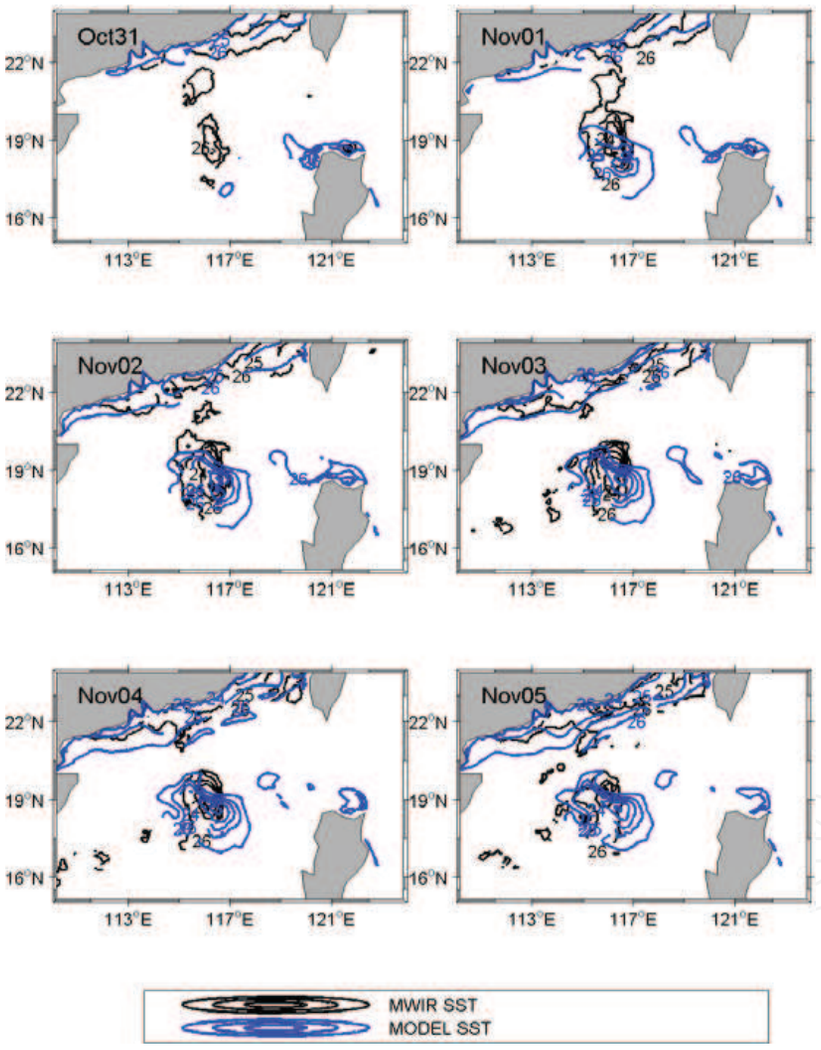

Figure 4. Isotherms of SST in the typhoon wake (unit: °C) from October 31 to November 5, 2006 (with the black lines showing the MWIR OI SSTs and blue lines showing the simulated SSTs).

Figure 4 shows the comparison of the daily surface isotherms between MWIR OI observations and the model simulations from October 31 to November 5. The isothermal lines ranged from 22°C to 26°C with 1°C intervals. The distributions of the simulated surface isotherms in the

http://dx.doi.org/10.5772/64099

wake area are quite consistent with the MWIR OI SSTs, which further demonstrate that the temperature simulations related to Typhoon Cimaron are well reproduced. The southward shift of the location of the maximum SST cooling in the simulation results compared to the satellite observations indicates another common issue during the forecasting of extreme weather conditions, which is the lack of high-accuracy wind forcing observations. The simulated maximum mixed layer depth was about 53.2 m, located at (18.51°N, 116.44°E) on November 3, 2006 which is an underestimate compared with the maximum deepening of 104.5 m at (19.50°N, 116.26°E) estimated in work [30]. Underestimation of the mixed layer depth and SST cooling is a common problem in the numerical ocean model simulations because of insufficient mixing. To solve this problem, a parameterization of wave-induced mixing is added to the model to improve the mixing estimates in this chapter (see details in Section 5).

4.2. Ocean currents

When Typhoon Cimaron entered the South China Sea on October 30, the upper ocean's response was almost instantaneous. Typhoon-induced cyclonic currents caused divergence of upper ocean water over the surface areas by tens of kilometres (in scale) with cold water that is upwelled from the deeper ocean, accounting for the formation of a cold-core eddy. The cyclonic currents flowed in a roughly circular motion around the mesoscale cold eddy, with the maximum velocity reaching 2.5 m s^{-1} at location (18.44°N, 115.3°E) on October 31. An alongshore current flowing through the Taiwan Strait into the South China Sea, driven by the northeast monsoon winds, was strengthened by the typhoon forcing on October 31 and November 1. The intrusion of Kuroshio Current meandering towards the South China Sea through the Luzon Strait was strengthened too, with the current velocity reaching 1.6 m s^{-1} north of the Philippines Islands on November 1.

A very large amount of potential and kinetic energy is injected into the ocean surface layer from the strong typhoon winds during the typhoon generation and development process. The power of the injected energy and the vorticity can be calculated using the following formulae:

$$W = \vec{F} \cdot \vec{U} = \tau_x u + \tau_y v \tag{1}$$

$$\zeta = \frac{\partial v}{\partial x} - \frac{\partial u}{\partial y} \tag{2}$$

where W represents the power in the units of W m^{-2}. Here, $\vec{F}$ represents the wind stress with (τ_x, τ_y) the two components corresponding to the (x, y) coordinates, respectively. $\vec{U}(u, v)$ is the simulated surface current velocity and ζ represents the vorticity.

Strong cyclonic currents caused by Typhoon Cimaron lasted for several days after typhoon's passage. Strengthened by the long-lasting intense typhoon wind forcing, the cyclonic eddy generated by the cyclonic circulation reached a maximum positive vorticity of 3.56×10^{-5} s^{-1} at the location (116.8°E, 18.3°N) on October 30, and continued intensifying to 5.36×10^{-5} s^{-1} on October 31 and 5.07×10^{-5} s^{-1} on November 1 (**Figure 5**). **Figure 6** shows estimates for the power

of the injected oceanic kinetic energy from October 30 to November 4. The power input from the wind forcing was mostly located on the right side of the typhoon's track with maxima of 1.45 W m^{-2} on October 31, and 1.43 W m^{-2} on November 1 and 0.54 W m^{-2} on November 2. The power input was low in the typhoon's eye area where the winds were very weak. The initial oceanic state was changed under the effect of the strong typhoon winds. On October 30, there is a large region with negative kinetic energy injected by the typhoon, appearing on the right side of the typhoon's track; this suggests that the oceanic kinetic energy was decreased by the typhoon. Thus, the intense typhoon winds changed the original pre-typhoon sea state conditions. The maximum decrease in the oceanic kinetic energy in the wake of the typhoon was 0.83 W m^{-2}. On October 31, the power reached a maximum value of 2.3 W m^{-2}, and on November 1, this value was 2.0 W m^{-2}.

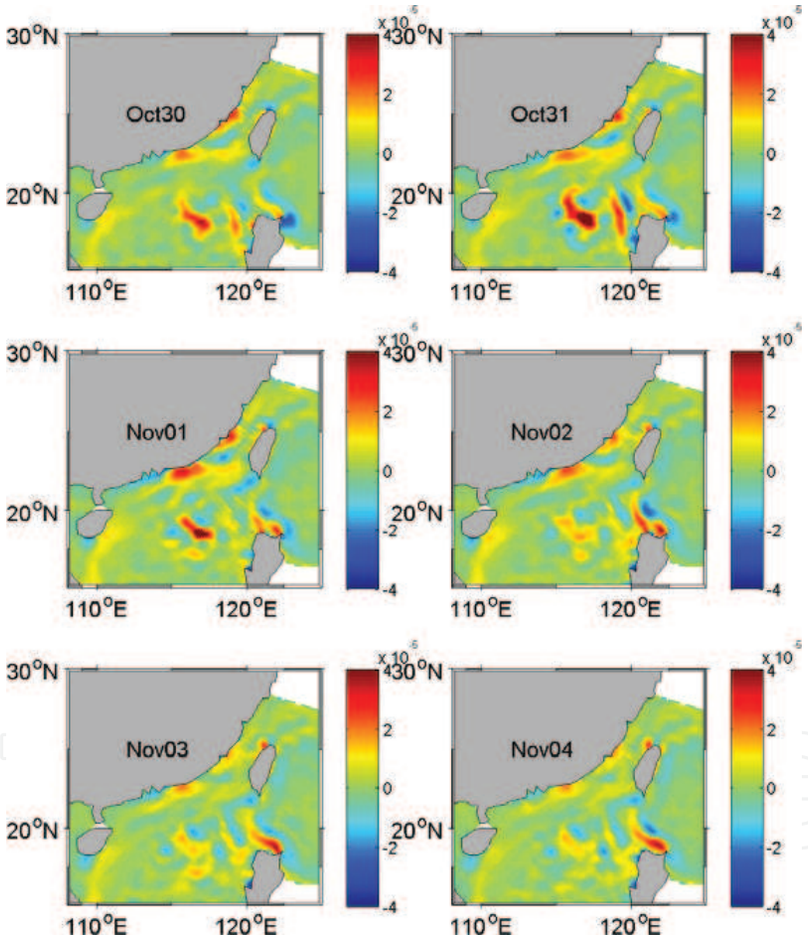

Figure 5. Surface vorticity from October 30 to November 4, 2006.

From November 2 onwards, the injected energy into the wake region of the typhoon showed the decreasing tendency pattern. However, the vorticity of the current induced by typhoon persisted for a long time after typhoon's passage. The study presented here shows that the energy input induced by the typhoon winds was responsible for the ocean-enhanced mixing processes.

http://dx.doi.org/10.5772/64099

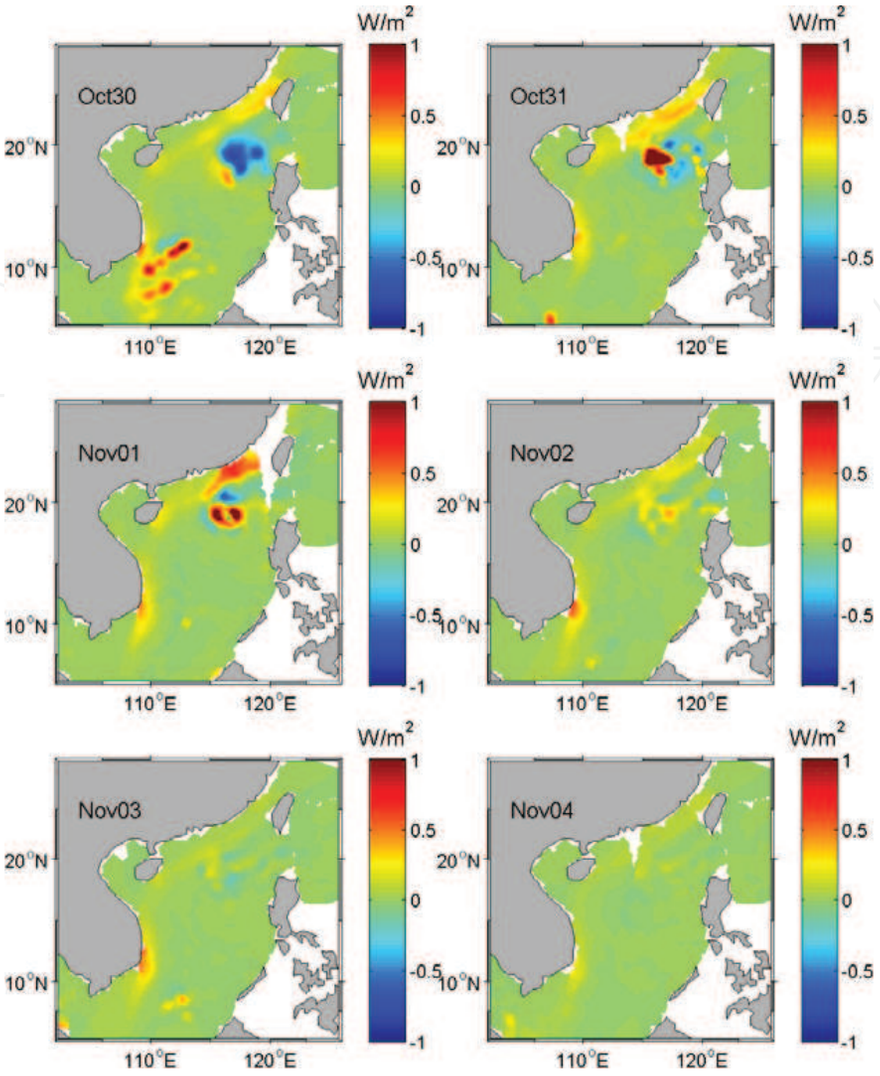

Figure 6. The power input to the ocean surface by the typhoon winds from October 30 to November 4, 2006.

4.3. Biological results

The monthly chlorophyll *a* concentration gridded datasets are obtained from the SeaWiFS observations, with a horizontal spatial resolution of 0.0417° × 0.0417°. **Figure 7** shows the monthly distributions of surface chlorophyll *a* concentration on October 16 and November 16, 2006 in the South China Sea. These two satellite images represent the pre- and post-typhoon situations for the primary production; it is evident that a phytoplankton bloom area exists around the location of the typhoon's wake after it had passed. Although the concentration of the chlorophyll *a* achieved high values, in excess of 4 mg cm^{-3} along the coast, the averaged concentration was about 0.09 mg cm^{-3} in the area that became the wake (the black box in **Figure 7**) before the appearance of Typhoon Cimaron. However, by November 16, the concentration in this area reached 0.85 mg cm^{-3}, which was much higher than the normal expected conditions, indicating that the maximum increase of chlorophyll *a* concentration was about 0.75 mg cm^{-3} at the location (17.02°N, 115.57°E) in the wake area. While the monthly

dataset may be interpolated in both spatial and temporal dimensions, the detailed processes related to the development of the phytoplankton bloom triggered by Typhoon Cimaron are still not clear. The application of the biological numerical model can provide more details for the study of the subsurface water layers and can complement the limitations of the satellite remote sensing.

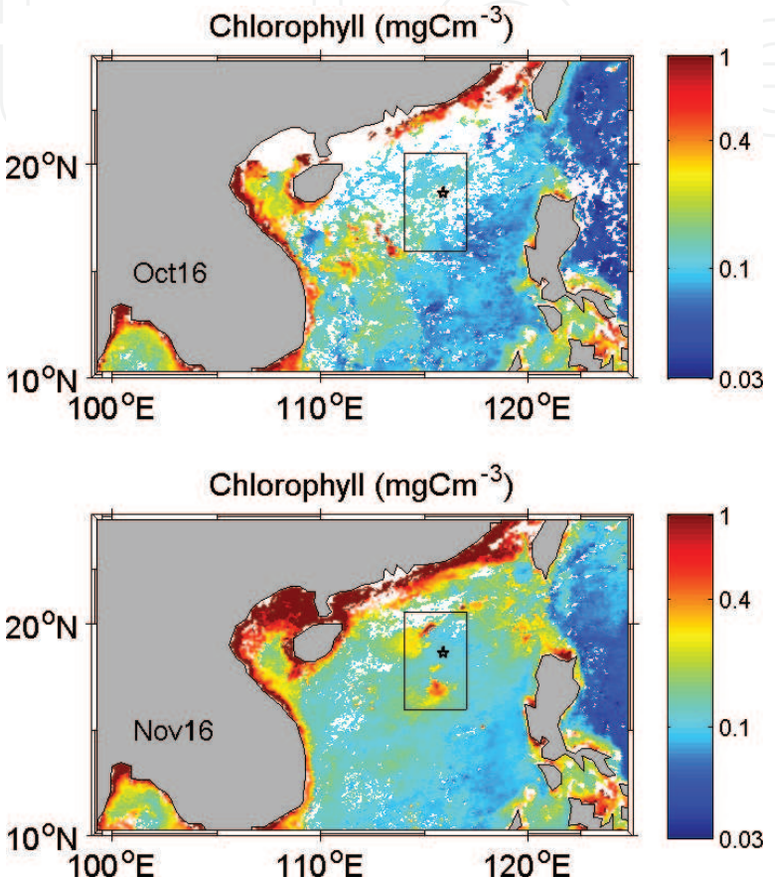

Figure 7. Chlorophyll *a* concentration (unit: mg cm^{-3}) from SeaWiFS on October 16 (upper panel) and November 16 (lower panel), 2006 (black box represents the areas in the wake of the typhoon; the pentagram marks the location used for calculation in **Figure 9**).

Figure 8 shows the simulated daily maximum surface concentrations of chlorophyll *a* and nitrate in the typhoon's wake area through October 28 to November 30. In the pre-typhoon condition, the nitrate concentration maintained a stable value of 0.03 mmol Nm^{-3}. During November 1–3, Cimaron lingered in locations that were quasistationary and caused strong mixing in the wave areas. Thus the nitrate concentration largely increased in the ocean surface layer in the wake, reaching a maximum of 1.24 mmol Nm^{-3} on November 3. By November 3, Cimaron had passed from this (wake) region. The surface nitrate concentration remained high, in excess of 1.1 mmol Nm^{-3} for an additional 3 days, from November 3–5, and then decreased to a rather stable level of 0.1 mmol Nm^{-3} from November 11 onwards.

Compared to the quick response of nitrate to Typhoon Cimaron, the response of the phytoplankton is a relatively slow process. The chlorophyll *a* concentration remained at the prety-

http://dx.doi.org/10.5772/64099

phoon level of about 0.06 mg cm^{-3} for some time beyond November 3. Although the mixed layer depth deepened to its maximum on November 3, the chlorophyll *a* concentration was still increasing at that time, having increased slightly over the previous 2 days, as triggered by the upwelling induced by the approaching storm. Thereafter, the chlorophyll *a* concentration increased rapidly in early November, reaching a rate of 0.5 mg cm^{-3} d^{-1}, and attaining a maximum concentration of 1.76 mg cm^{-3} on November 7. The phytoplankton blooms occurred 5 days after Typhoon Cimaron's passage. The chlorophyll *a* concentration began to decrease from November 8 onwards, returning to a quasistable level of 0.3 mg cm^{-3} by November 18. The maximum concentration of chlorophyll *a* on November 16 was simulated at the value of 0.65 mg cm^{-3}, which was about 0.2 mg cm^{-3} less than the satellite observations. The surface ocean was restored to an equilibrium state again by about 10–20 days after the interruption that Cimaron introduced. Moreover, the concentrations of both nitrate and chlorophyll *a* in the resulting re-equilibrium of the ocean state are higher than those of the former pre-typhoon state.

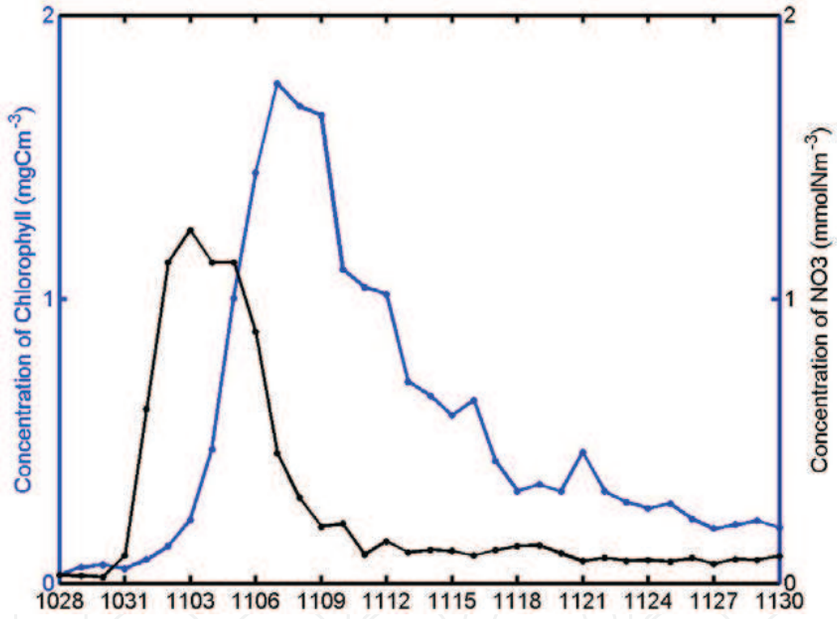

Figure 8. Simulated maximum concentrations of nitrate and chlorophyll *a* in the typhoon wake from October 28 to November 30, 2006.

The vertical profiles of the density, both of chlorophyll *a* and nitrate concentrations at the location (18.66°N, 115.89°E), as shown in **Figure 7**, in the typhoon wake are investigated with respect to the underwater impacts of Cimaron, comparing the pre- and post-typhoon profiles through October 28 to November 30 in **Figure 9**. Before the typhoon, the nutrient and phytoplankton in the surface layer are both at low concentrations, as the surface waters received strong light irradiation, which is not conducive to the growth and reproduction of the phytoplankton. Phytoplankton populations grow and reproduce mostly in the euphotic zone. The depth of the euphotic zone can be estimated from the chlorophyll *a* concentration of the surface layer, based on the assumption of Case-I waters; the equation is shown in [40]. After

the typhoon's passage, cyclonic eddies caused by Typhoon Cimaron exhibited the upward doming of isopycnals from October 31 and the isopycnals were uplifted with high nutrient concentrations into the euphotic zone, which furthermore, had a positive influence on the photosynthetic performance. The chlorophyll *a* concentration in the surface layer increased and reached about 0.237 mg cm^{-3} on November 7 in **Figure 9**. Both the profiles of nitrate and chlorophyll *a* are significantly elevated after the typhoon's passage. The euphotic zone depth was estimated as 87.0 m before typhoon and 36.2 m after typhoon in the wake, with respect to the chlorophyll *a* concentrations obtained from the satellite for pre- and post-typhoon Cimaron. The euphotic zone was uplifted by 50.0 m in the wake of Typhoon Cimaron.

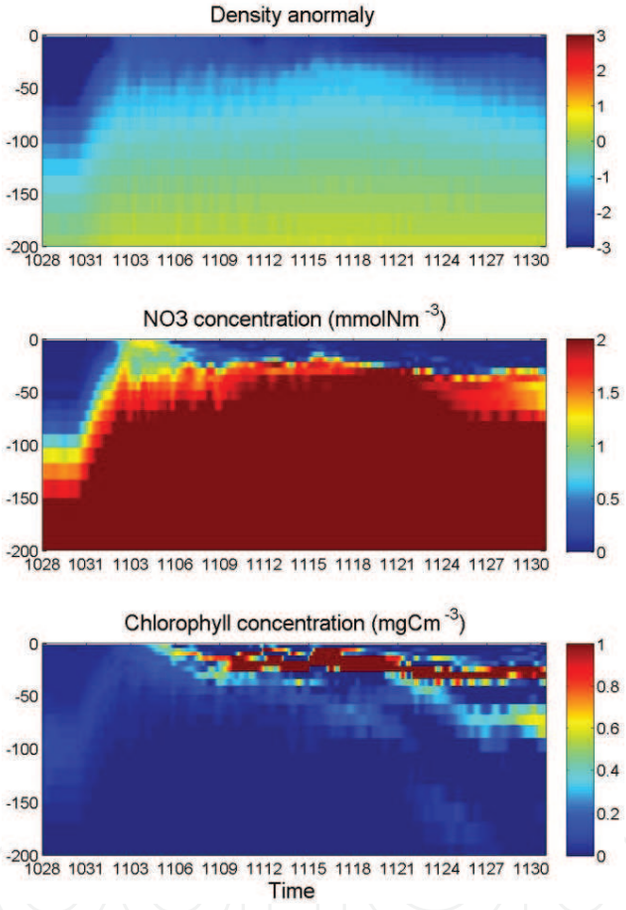

Figure 9. Profiles of chlorophyll *a* and nitrate concentration at the location (18.66°N, 115.89°E), shown in **Figure 7** in the typhoon wake from October 28 to November 30, 2006.

5. Discussion: effect of the wave-induced mixing

The mixed layer deepening induced by Typhoon Cimaron is underestimated in the three-dimensional ocean model simulations, which is a common situation in ocean model simulations. To strengthen the insufficient mixing, in our chapter, we incorporated the wave-induced

http://dx.doi.org/10.5772/64099

mixing term, B_V into ROMS to investigate the effect of B_V on the mixed layer deepening and ocean surface temperature cooling caused by Typhoon Cimaron.

The wave-induced mixing term B_V, is added into ROMS, as part of the vertical kinematic viscosity, as expressed by Qiao et al. [29]

$$B_V = \alpha \iint_{\vec{k}} E\left(\vec{k}\right)\exp\left(2kz\right)d\vec{k}\,\frac{\partial}{\partial z}\left[\iint_{\vec{k}} \omega^2 E\left(\vec{k}\right)\exp\left(2kz\right)d\vec{k}\right]^{1/2} \quad (3)$$

where ω is the wave angular frequency, z is the vertical coordinate axis downward positive with $z = 0$ at the surface, k is the wave number, and $E\left(\overrightarrow{k}\right)$ represents the wave number spectrum including both wind wave and swell waves. B_V can be calculated by the wave model. In this study, the wave-induced mixing term is directly derived from the Key Laboratory of Marine Science and Numerical Modeling (MASNUM) wave model [28] and is added into the vertical viscosity and diffusivity term of the K-profile parameterization (KPP) mixing scheme which is applied in ROMS. Because the wave mixing is dominant in the upper ocean layer, the B_V term is confined to the range from 1000 m depth up to the surface. The weighting coefficient was set to 0.1 in our study, as suggested by Wang et al. [41]. In the wake of the typhoon, the vertical mixing was strengthened with the vertical viscosity coefficient of 0.1 $m^2 s^{-1}$ from October 31 to November 2.

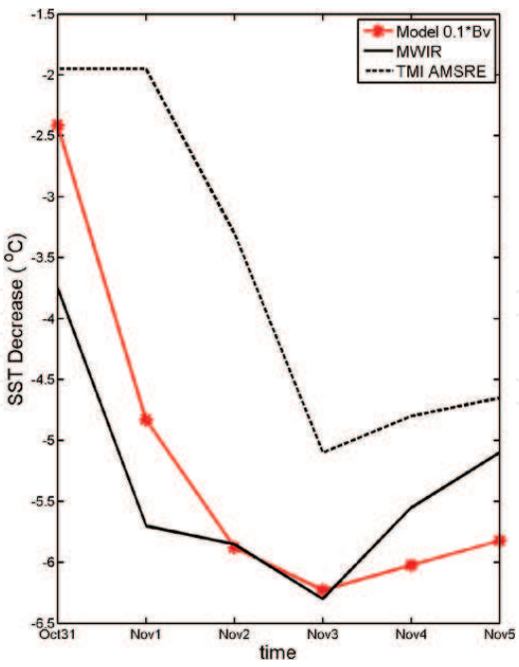

Figure 10. Maximum SST decrease in the wake from October 31 to November 5, 2006 (red solid line with asterisks denotes the model results; the dash line denotes TMI AMSRE satellite observations; the solid line represents MWIR satellite observations).

Figure 10 shows the maximum SST decrease in the wake of the typhoon, comparing the simulations by adding B_V with the two sets of satellite observations. Under the effect of the strengthened mixing estimates, SST in the wake reached the lowest temperature on November 3 with a value that is consistent with both sets of satellite observations. The maximum SST decreases on November 2 and November 3, respectively, relative to the pre-typhoon conditions on October 28, which were 5.9°C and 6.2°C, which are close to the MWIR observations of 5.8°C and 6.3°C. Compared to the maximum temperature decreases without the B_V term of 4.1°C on November 2 and 4.8°C on November 3 in the typhoon's wake, the wave-induced mixing can improve the SST cooling by 1.7°C on November 2 and 1.4°C on November 3. This is with a weighting coefficient of 0.1. The associated mixed layer deepening was increased by 30 m on November 3.

6. Conclusions

A three-dimensional simulation of the upper ocean in response to Typhoon Cimaron is investigated in this study, including both the physical and biological processes. The validation of SST was compared with two satellite observations, TMI AMSRE and MWIR OI SSTs, from October 30 to November 6. High correlation (over 84%) and low bias (between 0.4°C and 0.6°C) show that ROMS can reproduce the process of upper ocean response to Typhoon Cimaron quite well. Detailed analysis indicates that the surface cooling is underestimated due to the insufficient mixing in the ROMS model. To solve this problem, the wave-induced mixing with a certain weighting coefficient was introduced into the KPP mixing scheme to improve the simulation of SST cooling. Values up to 6.2°C are obtained, which is close to the observed MWIR cooling estimate of 6.3°C on November 3, whereas the ROMS simulation without the wave-induced mixing gives an underestimated cooling of 4.8°C. The simulation accuracy is enhanced by adding the wave-induced mixing, which increases the SST cooling by 1.4°C and deepens the mixed layer by 30 m in the wake of typhoon.

A strong mesoscale ocean eddy, as characterized by the cyclonic currents, was caused by Typhoon Cimaron in the South China Sea. The water within the eddy diverged over surface areas on a scale of tens of kilometres. Under the divergent condition, cold nutrient-rich water upwelled from deeper waters. The positive vorticity kept a high value over $5.0 \times 10^{-5}\ s^{-1}$ on October 31 and November 1. Moreover, the concentration of nitrate in the surface wake area increased to a maximum during these 2 days, which indicates that upwelling played a key role on the phytoplankton blooming after typhoon's passage. The simulated maximum concentration of chlorophyll *a* in the wake increased from a pre-typhoon value of 0.1 mg cm^{-3} to a post-typhoon value of 0.65 mg cm^{-3} on November 16, which is close to the satellite observation of 0.85 mg cm^{-3} on November 16. The euphotic zone was uplifted by 50.0 m after Typhoon Cimaron's passage. Thereafter, the ocean restored to a new equilibrium state with higher concentrations of chlorophyll *a* and nitrate than those existing in the pre-equilibrium state in the wake area.

Acknowledgements

We thankfully acknowledge funding support from the General Research Fund of Hong Kong Research Grants Council (RGC) under Grants CUHK 402912 and 403113, the Hong Kong Innovation and Technology Fund under the Grants of ITS/321/13, the direct grants of the Chinese University of Hong Kong, the National Natural Science Foundation of China under project 41376035, the Marine Environmental Observation Prediction and Response Network (MEOPAR), DFO's Aquatic Climate Change Adaptation Service (ACCASP), the PERD, and the Canadian Panel on Energy Research and Development.

Appendices

Appendix A – Acronyms

B_V	Wave-induced mixing
K1	Lunisolar declinational diurnal tidal constituent
K2	Lunisolar declinational semidiurnal tidal constituent
KPP	K-profile parameterization
M2	Principal lunar semidiurnal tidal constituent
MAE	Mean absolute error
MASNUM	Key Laboratory of Marine Science and Numerical Modeling
ME	Mean error
Mf	Lunar fortnightly long-period tidal constituent
Mm	Lunar monthly long-period tidal constituent
MWIR OI	Microwave infrared optimally interpolated
N2	Larger lunar elliptic semidiurnal tidal constituent
NH_4	Ammonium
NO_3	Nitrate
R	Correlation coefficient
RMS	Root-mean-square
ROMS	Regional Ocean Modeling System
S2	Principal solar semidiurnal tidal constituent
SeaWIFS	Sea-Viewing Wide Field-of-View Sensor
SSTs	Sea surface temperatures
SODA	Simple Ocean Data Assimilation dataset

TIC	Total inorganic carbon
TMI AMSRE	Tropical Rainfall Measuring Mission (TRMM) Microwave Imager and Advanced Microwave Scanning Radiometer
TPXO	The OSU TOPEX/Poseidon Global Inverse Solution
O1	Principal lunar diurnal tidal constituent
OAFlux	Objectively Analyzed air-sea Fluxes
P1	Principal solar diurnal tidal constituent
POM	Princeton Ocean Model
Q1	Major lunar elliptical diurnal tidal constituent
QuikSCAT	NASA Quick Scatterometer Earth observation satellite
WOA01	World Ocean Atlas 2001
WOA09	World Ocean Atlas 2009

Author details

Yujuan Sun[1,2,3], Jiayi Pan[1,4,5*] and William Perrie[2,3]

*Address all correspondence to: panj@cuhk.edu.hk

1 Institute of Space and Earth Information Science, The Chinese University of Hong Kong, Hong Kong, China

2 Department of Engineering Mathematics and Internetworking, Dalhousie University, Halifax, Nova Scotia, Canada

3 Fisheries and Oceans Canada, Bedford Institute of Oceanography, Dartmouth, Nova Scotia, Canada

4 Shenzhen Research Institute, The Chinese University of Hong Kong, Shenzhen, China

5 School of Marine Science, Nanjing University of Information Science and Technology, Nanjing, Jiangsu, China

References

[1] Gill AE: On the behavior of internal waves in the wakes of storms. J. Phys. Oceanogr. 1984; 14: 1129–1151.

[2] Price JF, Sanford TB, Forristall GZ: Forced stage response to a moving hurricane. J. Phys. Oceanogr. 1994; 24: 233–260.

[3] Leipper DF: Observed ocean conditions and Hurricane Hilda 1964. J. Atmos. Sci. 1967; 24: 182–196.

[4] Bolin B: The adjustment of a non-balanced velocity field towards geostrophic equilibrium in a stratified fluid. Tellus. 1953; 5(3): 373–385.

[5] Pollard RT: On the generation by winds of inertial waves in the ocean. Deep-Sea Res.. 1970; 17(4): 795–812. DOI: 10.1016/0011-7471(70)90042-2.

[6] Veronis G: Partition of energy between geostrophic and non-geostrophic oceanic motions. Deep-Sea Res.. 1956; 3(3): 157–177. DOI: 10.1016/0146-6313(56)90001-6.

[7] Pollard RT, Millard Jr RC: Comparison between observed and simulated wind-generated inertial oscillations. Deep-Sea Res.. 1970; 17(4): 813–821. DOI: 10.1016/0011-7471(70)90043-4.

[8] Blumen W, Wu R: Geostrophic adjustment: frontogenesis and energy conversion. J. Phys. Oceanogr. 1995; 25: 428–438.

[9] Geisler JE: Linear theory of the response of a two layer ocean to moving hurricane. Geophys. Fluid Dyn. 1970; 1: 249–272. DOI: 10.1080/03091927009365774.

[10] Ginis I, Sutyrin G: Hurricane-generated depth-averaged currents and sea surface elevation. J. Phys. Oceanogr. 1995; 25: 1218–1242.

[11] Black PG: The 3D oceanic mixed layer response to Hurricane Gilbert. J. Phys. Oceanogr. 2000; 30: 1407–1429.

[12] Chang J, Chung CC, Gong GC: Influences of cyclones on chlorophyll *a* concentration and Synechococcus abundance in a subtropical western Pacific coastal ecosystem. Mar. Ecol. Prog. Ser. 1996; 140: 199–205.

[13] Hung CC, Gong GC, Chou WC, Chung CC, Lee MA, Chang Y, Chen HY, Huang SJ, Yang Y, Yang WR, Chung WC, Li SL, Laws E: The effect of typhoon on particulate organic carbon flux in the southern East China Sea. Biogeosciences. 2010; 7: 3007–3018.

[14] Babin SM, Carton JA, Dickey TD, Wiggert JD: Satellite evidence of hurricane-induced phytoplankton blooms. J. Geophys. Res. 2004; 109: C03043. DOI: 10.1029/2003JC001938.

[15] Lin I, Liu W, Wu CC, Wong TF, Hu C, Chen Z, Liang WD, Yang Y, Liu KK: New evidence for enhanced ocean primary production triggered by tropical cyclone. Geophys. Res. Lett. 2003; 30(13). DOI: 10.1029/2003GL017141.

[16] Zheng G, Tang D: Offshore and nearshore chlorophyll increases induced by typhoon winds and subsequent terrestrial rainwater runoff. Mar. Ecol. Prog. Ser. 2007; 333: 61–74.

[17] Shang S, Li L, Sun F, Wu J, Hu C, Chen D, Ning X, Qiu Y, Zhang C, Shang S: Changes of temperature and bio-optical properties in the South China Sea in response to

Typhoon Lingling 2001. Geophys. Res. Lett. 2008; 35: L10602. DOI: 10.1029/2008GL033502.

[18] Zhao H, Tang D, Wang Y: Comparison of phytoplankton blooms triggered by two typhoons with different intensities and translation speeds in the South China Sea. Mar. Ecol. Prog. Ser. 2008; 365: 57–65.

[19] Chang Y, Liao HT, Lee MA, Chan JW, Shieh WJ, Lee KT, Wang GH, Lan YC: Multisatellite observation on upwelling after the passage of Typhoon Hai-Tang in the southern East China Sea. Geophys. Res. Lett. 2008; 35: L03612. DOI: 10.1029/2007GL03285.

[20] Franks PJS, Wroblewski JS, Flierl GR: Behavior of a simple plankton model with food-level acclimation by herbivores. Mar. Biol. 1986; 91: 121–129.

[21] Fennel K, Wilkin J, Levin J, Moisan J, O'Reilly J, Haidvogel D: Nitrogen cycling in the Middle Atlantic Bight: results from a three-dimensional model and implications for the North Atlantic nitrogen budget. Global Biogeochem. 2006; 20: GB3007. DOI: 10.1029/2005GB002456.

[22] Powell TM, Lewis CVW, Curchitser EN, Haidvogel DB, Hermann AJ, Dobbins EL: Results from a three-dimensional, nested biological-physical model of the California Current System and comparisons with statistics from satellite imagery. J. Geophys. Res. 2006; 111: C07018. DOI: 10.1029/2004JC002506.

[23] Ezer T: On the seasonal mixed layer simulated by a basin-scale ocean model and the Mellor-Yamada turbulence scheme. J. Geophys. Res. 2000; 105: 16843–16855.

[24] Mellor G: The three-dimensional current and surface wave equations. J. Phys. Oceanogr. 2003; 33: 1978–1989.

[25] Sanford TB, Black PG, Haustein JR, Feeney JW, Forristall GZ, Price JF: Ocean response to a hurricane. Part I: observations. J. Phys. Oceanogr. 1987; 17: 2065–2083.

[26] Craig PD, Banner ML: Modeling wave-enhanced turbulence in the ocean surface layer. J. Phys. Oceanogr. 1994; 24: 2546–2559.

[27] Mellor G, Blumberg A: Wave breaking and ocean surface layer thermal response. J. Phys. Oceanogr. 2004; 34: 693–698.

[28] Yuan Y, Qiao F, Hua F, Wan Z: The development of a coastal circulation numerical model: I. Wave-induced mixing and wave-current interaction. J. Hydrodyn. Ser. A. 1999; 14: 1–8.

[29] Qiao F, Yuan Y, Yang Y, Zheng Q, Xia C, Ma J: Wave-induced mixing in the upper ocean: distribution and application to a global ocean circulation model. Geophys. Res. Lett. 2004; 31: L11303. DOI: 10.1029/2004GL019824.

[30] Pan J, Sun Y: Estimate of ocean mixed-layer deepening after a typhoon passage over the South China Sea by using satellite data. J. Phys. Oceanogr. 2013; 43: 498–506.

[31] Carton JA, Giese BS: A reanalysis of ocean climate using Simple Ocean Data Assimilation (SODA). Mon. Weather Rev. 2008; 136: 2999–3017.

[32] Egbert GD, Bennett AF, Michael MGG: TOPEX/POSEIDON tides estimated using a global inverse model. J. Geophys. Res.. 1994; 99(C12): 24821–24852.

[33] Yu L, Jin X, Weller RA: Multidecade global flux datasets from the Objectively Analyzed Air-sea Fluxes (OAFlux) project: latent and sensible heat fluxes, ocean evaporation, and related surface meteorological variables, Woods Hole Oceanographic Institution, OAFlux Project Technical Report, OA-2008-01. Woods Hole, Massachusetts; 2008. 64 p.

[34] Haney RL: Surface thermal boundary condition for ocean circulation models. J. Phys. Oceanogr. 1971; 1: 241–248.

[35] Garcia HE, Locarnini RA, Boyer TP, Antonov JI, Baranova OK, Zweng MM, Johnson DR. World Ocean Atlas 2009, Volume 3: Dissolved Oxygen, Apparent Oxygen Utilization, and Oxygen Saturation. S. Levitus, Ed. NOAA Atlas NESDIS 70, U.S. Government Printing Office, Washington D.C.; 2010. 344 p.

[36] Garcia HE, Locarnini RA, Boyer TP, Antonov JI, Zweng MM, Baranova OK, Johnson DR: World Ocean Atlas 2009, Volume 4: Nutrients (phosphate, nitrate, silicate). S. Levitus, Ed. NOAA Atlas NESDIS 71, U.S. Government Printing Office, Washington D.C.; 2010. 398 p.

[37] Morel A, Berthon JF: Surface pigments, algal biomass profiles, and potential production of the euphotic layer: relationships reinvestigated in view of remote-sensing applications. Limnol. Oceanogr. 1989; 34: 1545–1562.

[38] Goyet C, Healy RJ, Ryan JP: Global distribution of total inorganic carbon and total alkalinity below the deepest winter mixed layer depths. 2000; NDP-076, http://cdiac.ornl.gov/oceans/ndp_076/.

[39] Sun Y, Qiao F, Wang G, Ying X, Yang Y: Forecast operation and verification of MASNUM surface wave numerical model (in Chinese). Adv. Mar. Sci.. 2009; 27(3): 281–293.

[40] Lee Z, Weidemann A, Kindle J, Arnone R, Carder KL, Davis C: Euphotic zone depth: its derivation and implication to ocean-color remote sensing. J. Geophys. Res. 2007; 112: C03009. DOI: 10.1029/2006JC003802.

[41] Wang Y, Qiao F, Fang G, Wei Z: Application of wave-induced vertical mixing to the K profile parameterization scheme. J. Geophys. Res. 2010; 115: C09014. DOI: 10.1029/2009JC005856.

IntechOpen